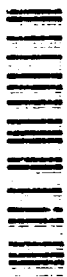


AD-A270 862



WHOI-93-22

2

# Woods Hole Oceanographic Institution



## A Laboratory Model of a Cooled Continental Shelf

by

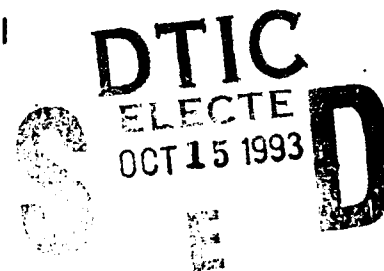
J.A. Whitehead and Robert E. Frazel

June 1993

### Technical Report

Funding was provided by the Office of Naval Research  
under Contract No. N00014-89-J-1037.

Approved for public release; distribution unlimited.



93-24119



90 10 12 102

**WHOI-93-22**

**A Laboratory Model of a Cooled Continental Shelf**

by

J.A. Whitehead and Robert E. Frazel

Woods Hole Oceanographic Institution  
Woods Hole, Massachusetts 02543

June 1993

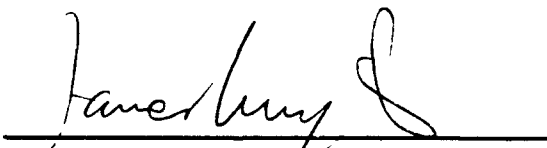
**Technical Report**

Funding was provided by the Office of Naval Research  
under Contract No. N00014-89-J-1037.

Reproduction in whole or in part is permitted for any purpose of the United States Government. This report should be cited as Woods Hole Oceanog. Inst. Tech. Rept., WHOI-93-22.

Approved for public release; distribution unlimited.

**Approved for Distribution:**

  
**James Luyten, Chair**  
Department of Physical Oceanography

## Table of Contents

## Page

Abstract	i
1. Introduction and Literature Review	1
2. The Experimental Apparatus	3
3. Structure of the Temperature and Flow Field	4
4. Heat Flow Measurements	8
Acknowledgements	32
References	33

## List of Figures

1. Sketch of apparatus and layout of thermistors.	4
2. Temperature section along a radial line from the coast to the center.	5
3. Temperature as a function of time for a typical experiment	8,9
4. Measurements in the preliminary experiments of heat flow and temperature difference with time	11
5. Temperature versus time for final thermistor placement.	12
6. Temperature difference between thermistors 2 through 6 and 9, versus time.	13
7. Heat flux estimates for thermistors 2, 4, 5, 6, and 9.	14
8. Heat flux versus temperature difference for thermistors 2 through 6.	15
9. Temperature versus time for baffled and nonbaffled experiments.	16
10. Heat flux versus temperature difference for baffled and nonbaffled results.	17
11. Heat flux versus temperature difference for the 5 cm deep experiments.	19
12. Heat flux versus temperature for experiments with baffled lid and 10 cm depth.	20
13. Heat flux versus temperature for experiments with nonbaffled lid and 10 cm depth.	21
Figure 14. Heat flux versus temperature for experiments with a nonbaffled lid and 20 cm depth.	22
Figure 15. Best fit lines for data shown in Fig. 13b.	27
Figure 16. Temperature difference versus rotation rate for experiments with heat flux of approximately 100 cal/s and 10 cm depth.	28
Figure 17. a. All measured values of $D_4$ and $D_5$ versus $DT_h$ . b. Same in logarithm scale.	30
c. Same as 17b but each depth denoted by a different symbol	31
Figure 18. Measured values of $D_4$ and $D_5$ versus predicted various terms in equation (6)	32

## List of Tables

Table 1. Rotation rate, temperature difference ( $^{\circ}\text{C}$ ) and heat flux (cal/s) for the 5 cm deep shelf baffled experiments	23
Table 2. Rotation rate, temperature difference ( $^{\circ}\text{C}$ ) and heat flux (cal/s) for the 10 cm deep baffled shelf experiments	24
Table 3. Rotation rate, temperature difference ( $^{\circ}\text{C}$ ) and heat flux (cal/s) for the 10 cm deep shelf nonbaffled experiments	25
Table 4. Rotation rate, temperature difference ( $^{\circ}\text{C}$ ) and heat flux (cal/s) for the 20 cm deep nonbaffled shelf experiments	26

## Abstract

A laboratory model of wintertime cooling over a continental shelf has a water surface cooled by air in an annular rotating tank. A flat shallow outer "continental shelf" region is next to a conical "continental slope" bottom and a flat "deep ocean" center. The shelf flow consists of cellular convection cells descending into a region with very complicated baroclinic eddies. Extremely pronounced fronts are found at the shelf break and over the slope. Associated with these are sizable geostrophic currents along the shelf and over shelf break contours. Eddies are particularly energetic there. Cooling rate is compared with temperature difference between "continental shelf" and "deep ocean". Scaling considerations produce an empirical best fit formula for temperature difference as a function of cooling rate. This produces a relatively straight regression line over a wide range of rotation rates, shelf depths and cooling rates. If this formula is valid for the ocean, water over continental shelves will be much colder due to constraints imposed by rotation of the earth than if the fluid were not rotating.

Key words: Cooled shelf, continental shelf, laboratory model, convection

Accession For	
NTIS CRA&J	<input checked="checked" type="checkbox"/>
DTIC TAB	<input checked="checked" type="checkbox"/>
Unannounced	<input type="checkbox"/>
Justification _____	
By _____	
Distribution _____	
Availability Codes	
Dist	Avail and/or Special
A-1	

# **1. Introduction and Literature Review**

The densest water in the ocean is found at the bottom of polar seas. To acquire that density, surface water experienced either temperature decrease through cooling or salinity increase by evaporation or ice formation. Sinking on a continental shelf proceeds when water cooled on the shelf accumulates until pools of dense water get large enough to seek channels to the bottom. Water flowing away from the region of formation becomes impeded by fronts with geostrophic flow at right angles to the pressure gradient. Water flowing in to replace the outflow of dense water is also influenced by rotation. The final flux depends on either bathymetric channels, Ekman layer transport, or eddies from cross-frontal instability. Once the dense water crosses the shelf break, it sinks to the bottom along a density current on the continental slope.

Estimates of the rate of flow off the shelf as a function of temperature difference can be calculated for constant depth shelves using theoretical models of rotating cross-shelf transport like those of Stommel and Leetmaa (1972), Csanady (1976), and Whitehead (1981). In these models, the dense fluid is removed from the shelf by seaward flow in the bottom Ekman layer and replaced by shoreward flow in the top Ekman layer. Estimates of cross-shelf transport rates in the above three studies were made only for a shelf of constant depth. Unfortunately, the flows themselves are baroclinically unstable for most ocean circumstances (Whitehead 1981) so the estimates may be unrealistic. In a computer model by Hsu (private communication) calculations of cross-shelf transport in the Ekman layer were done for a shelf with sloping bottom. It is not known whether that flow is unstable to three dimensional disturbances. The flux was determined for a few cases. In all cases some estimate of the rate of transport of the basic states was obtained. It is not known whether these rates are overshadowed by transport from eddies, or limited by dynamics of the front at the shelf edge. Another rate limiting process is found on the front at the edge of the continental shelf. Killworth (1977) explored the structure and the downstream consequences of the front. Models with behavior like the ocean were produced by adopting appropriate mixing coefficients.

An experiment and simple theory was conducted by Sugimoto and Whitehead (1983) for a rotating bay-type of shelf. The tank consisted of a shallow rectangular bay bordered on three sides by vertical walls and on the fourth by a steep sloping bottom that connected the bay to a deep offshore basin. The offshore side of the deep basin was a

metal wall connected to a thermostatic hot bath. The top surface of the water was in contact with a Plexiglas lid flushed by cold water, so the entire basin was subjected to surface cooling. The heat flow law in the limit of fast rotation was thought to be provided by the geostrophic flow of the currents entering and leaving the shallow bay. The currents lean on the sidewalls that stretch across the model continental shelf from coast to offshore. Experimental verification for the functional form of this law was found but the constant of proportionality was not fully explained. A numerical study of a cooled rectangular bay by Killworth (1974) was comprised of two layers with changing density. The results were plausible, but it was not conducted over a large range of parameters so parametric results cannot be compared with the above theories.

Studies that ignore rotation apply to smaller estuarine regions. Endoh (1977) constructed a model of cooling of a step-like shelf with both salt and thermal forcing and found the formation of a thermohaline front at the edge of the shelf. Kowalik and Matthews (1983) conducted a numerical study of a nonrotating bay type of shelf. They recovered a velocity magnitude of 1 cm/s and a realistic density distribution, but there was no search through governing parameter space that would allow the results to be applied to other problems. Brocard et al. (1977) and Brocard and Harleman (1980) intended to model flushing in side arms of cooling lakes. In their theoretical formulation the flushing mechanism was expressed using a two layer formulation where warm surface water flowed into the cooling lake. It then descended by surface cooling in a mixed region beyond a singular point where Froude number  $u/(g'h_1)^{1/2}$  equaled a given value and flowed out along the bottom. In this formula,  $u$  is velocity of the water onto the cooling lake,  $h_1$  is depth of the layer, and  $g'$  is gravity  $g$  times density difference between the cold water and the warm water, normalized by average density of the water. The speed of the flow was limited by turbulent friction. Laboratory experiments were used to verify the law relating heat flux with the temperature difference between offshore and the lake. There was satisfactory agreement between the law and the observations. A specific formula from this law subject to one simplifying assumption is given in section 6 of Whitehead (1993).

This formula is very similar to formulas arising from a second group of calculations that ignore friction entirely, but limit the speed of the flow by inertia. The theory used for these calculations has many names such as overmixing (Stommel and Farmer 1952a,b and Bryden and Stommel 1984), lock-exchange (Wood 1970) and maximal exchange (Farmer and Armi 1986). Predictions relating heat flux and temperature difference between

offshore and the deep region can also be determined using other studies of two-layer critically controlled flows as given for instance by Yih (1980) or Armi (1986). In most cases there is approximate agreement between the formulas and laboratory results. These formulas will be used to test the laboratory results, which are the topic of this report.

## **2. The Experimental Apparatus**

Our objective is to investigate relations between temperature difference (shelf to offshore) and heat flux for the laboratory equivalent of very long continental shelves. It was desired to eliminate sidewalls from coast to offshore since these were seen by Sugimoto and Whitehead to support cross-shelf geostrophic currents. To accomplish this, an annular geometry was used. A cylindrical tank was fitted with a shallow but wide polyvinylchloride (pvc) shelf along its outer perimeter as shown in Fig. 1. The inside radius of this shelf was 52.7 cm and the outside radius was 80.25 cm. Bordering the shelf on the outside was a 25 cm high vertical wall. Bordering it on the inside was a sloping conical pvc bottom with a 45 degree slope that descended to a deep flat fiberglass bottom of radius 25 cm. The horizontal bottoms of the tank were leveled so that depths were level to better than 2 mm everywhere. The outside of the tank was covered by one inch foam thermal insulation to retard conductive heat transfer to the room through the walls and bottom of the tank. The tank was mounted on the two meter turntable at the Coastal Research Center of Woods Hole Oceanographic Institution. This turntable is capable of angular rotation speeds  $2\Omega = \dot{\phi}$  of 0.008 to  $1 \text{ s}^{-1}$ .

Streak photographs, dye trajectories and temperature measurements from emplaced temperature probes constituted the data gathering activities. Thermistors used were 3000 ohm Omega brand precision thermistors that were read directly on an ohmmeter. The thermistors were calibrated in baths at 20, 25, 30, and 35°C (temperature was measured with a mercury thermometer calibrated to 0.01°C) and a fit was made to a third degree polynomial. The absolute value of the temperature calibration curve differed from the manufacturer's numbers by up to 0.3°C, which exceeds their claim of 0.1° accuracy, but the precision of temperature differences over a ten degree span was better than 0.1°C (the greatest difference used was about 6°C).

The tank was filled with hot tap water (of order 45°C) in the morning and the apparatus was left rotating all day. As the water cooled off (from sensible and evaporative

cooling to the room), colder water would accumulate on the shelf rather than at the middle and a convectively driven flow would be set up.

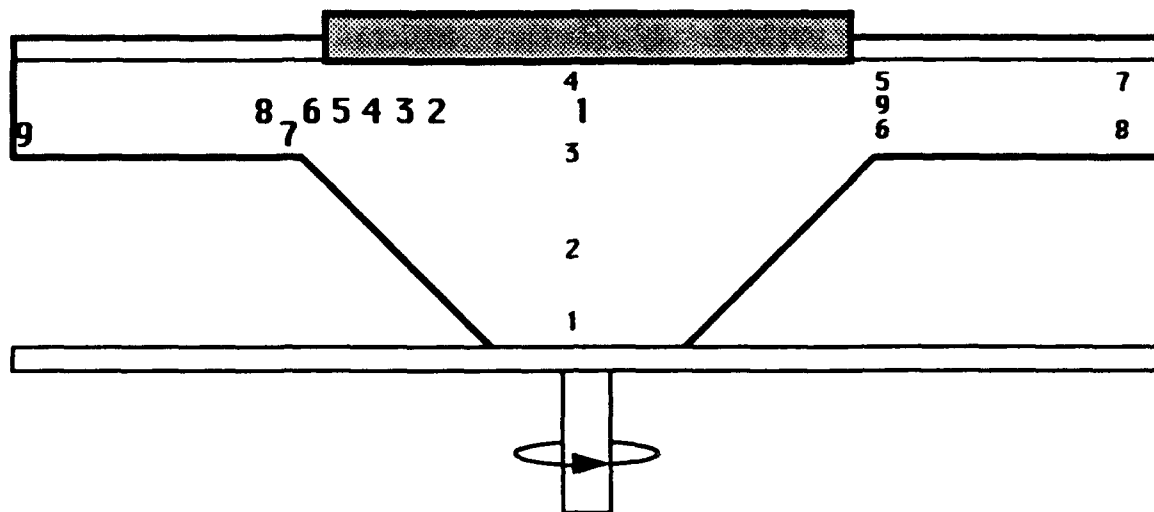


Figure 1. Sketch of apparatus and layout of thermistors. The thermistor locations shown in small numbers are for the exploratory experiments, and those shown by larger numbers are for the final experiments. The gray cover on the top center is Styrofoam. The tank was insulated on the sides and bottom.

### 3. Structure of the Temperature and Flow Field

The purpose of this section is to give a qualitative and crude quantitative image of the temperature and flow field. A typical temperature section along a radial line from the outer wall to the center is shown in Fig. 2. In this experimental run there was no insulation on the top surface so surface cooling was constant everywhere. Depth of the water on the shelf was 10 cm, the rotation rate  $f=1.000 \text{ s}^{-1}$ , and the experiment had been running for about three hours when the section was taken. One can consult figures showing evolution of the temperature field in the following sections to see that it is likely that the temperature field had become quasi-steady after about two hours. The data were acquired by thermistor readings at eight vertical lines (stations) at distances from the outer wall of 0, 10, 20, 30, 35, 40, 60, and 80 cm. Readings were taken at depths of 0, 2, 4, 6, 8, 10, 15, 20, 25, 30 and 35 cm or until the bottom was touched.

Near the center of the tank, Fig. 2 reveals there is a large region of water with temperature above  $32^{\circ}\text{C}$ . The temperature only decreases slightly with depth except for a



region a few centimeters off the bottom where a sharper decrease is found. Temperature also gradually decreases as one moves toward the shelf at all levels. This central region has the lowest temperature gradients of anywhere and the isotherms are bowl-shaped. Over the sloping region, a greater temperature gradient roughly 10 cm above the slope indicates a shelf front. Dye was injected at two levels in this region near the break to get a crude measurement of the speed of the mean along-shelf currents. There is an extremely strong baroclinic shear, with water flowing toward the viewer at a speed of about  $0.1 \text{ cm s}^{-1}$  near the bottom and away from the viewer at a speed of about  $0.5 \text{ cm s}^{-1}$  at the top. Evidence of many eddies around and within this front was seen in the dye trajectories. This front is one of the most important features of both the flow and thermal structure in the experiment. Over the flat shelf there is a tilt of isotherms like over the slope, but the isotherms are further apart. There was a movement of injected dye on the shelf away from the viewer with a speed of about  $0.05 \text{ cm s}^{-1}$ .

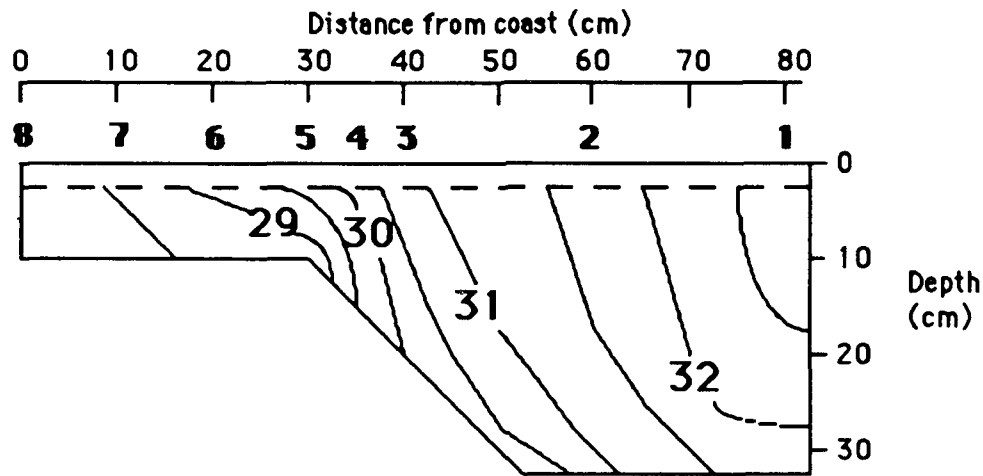


Figure 2. A temperature section along a radial line from the coast (left) to the center (right) after cooling for about three hours. Isotherms are shown in intervals of  $0.5^\circ\text{C}$ . The top mixed layer is above the dashed line.

These velocities are consistent with a thermal wind balance using

$$f \frac{\partial v}{\partial z} = -\frac{g}{\rho} \frac{\partial \rho}{\partial x} \quad (1)$$

where  $z$  is the vertical direction,  $x$  increases from left to right in Fig. 2, and  $v$  is positive away from us. For the frontal region, using for density  $\rho = \rho_0(1 - \alpha T)$ , where  $\alpha = 2 \times 10^{-4} \text{C}^{-1}$  and taking both  $x$  and  $z$  scales to be 10 cm, we estimate from Fig. 2 that there is a lateral temperature change of 2 degrees over 10 cm in the front region. This gives an along-shelf velocity change of 0.4 cm/s over a vertical distance of 10 cm, a value somewhat lower than our observed velocity change of 0.6 cm/s between the top of the shelf break and the bottom. On the shelf a 0.4 degree temperature change in 10 cm is reasonable. This gives a predicted vertical change of velocity of  $0.08 \text{ cm s}^{-1}$ . Assuming velocity is zero at the bottom boundary of the shelf, we predict 0.08 cm/s at the very top of the 10 cm deep water. This is roughly the 0.05 cm/s estimated from the dye, which was conveyed up and down by convection and geostrophic turbulence so that it did not apply to any particular depth.

For most runs, the flow was very irregular and characterized by baroclinic eddies superimposed on the drifts estimated above. Starting from offshore, the density current descended to the bottom of the tank where it tended to break up into irregular blobs. Above these blobs was intense cyclonic eddy activity, similar to that described by Whitehead, Stern, Flierl, and Klinger (1990). The cyclones were so strong that dimples were often easily seen on the top free surface of the water. On the shelf itself there were two eddy scales. The larger of the two consisted of circular conical blobs of cold water that has accumulated from surface cooling. These blobs are surrounded by wisps of dye that tended to move around. It was not possible to identify individual blobs for a long enough time to see whether they gradually got to the shelf break and fell off the edge before changing their shape, or whether instead they changed many times before the cold water found its way to the edge of the break. The second scale was from convection cells. These consisted of inverted plumes of cold surface water sinking to the bottom. They are revealed as white circular holes in the dye. Although the two scales seemed similar in size, for slow rotation rates the baroclinic eddy scale was much larger than the convection scale. The overall pattern of flows is similar to that described in Sugimoto and Whitehead. When the internal Rossby radius of deformation was as large as the width of the shelf, there tended to be large baroclinic eddies on the shelf. These possessed patches of convection cells in preferential regions. Around these eddies, sinuous jetlike fronts often appeared to wander from the inner wall to over the shelf break. They are similar to those seen in annulus experiments (Fultz 1961, Hide and Mason 1975). The dye revealed that fronts

(both on the shelf and over the shelf break) generally penetrated from surface to bottom so the eddies had a strong barotropic component in addition to their baroclinic nature. Only when rotation was very slow did the eddies of dense water appear to be bottom trapped and surface water top trapped. The measurement of eddy scale was beyond the scope of this project, so no information is available as to the scale of eddies as a function of the experimental parameters.

Streak photographs were taken of surface flow in experiments with no Styrofoam lid. In the central "deep ocean" region is a circulation that is rapid and relatively steady. Standing in the laboratory, we saw that the flow had almost no rotation. Thus in the rotating frame the flow is anticyclonic. This circulation arises because of the upwelling of warm water in the deep basin since it is being replenished from below by cooled water from the shelf, and is flowing onto the shelf at the surface to replace that cooled water. This very rapid offshore current is undesirable since oceans do not have them (it is a consequence of the smallness of the deep basin of the apparatus). Moreover, circulation is clearly associated with the bowl shaped isotherms in Fig. 2 since fluid in the deeper regions of the central "deep ocean" is less retrograde (because it is not flowing onto the shelf and thus is less divergent). These isotherms made it difficult to decide where the offshore edge of the front was. There is also a sharp lateral shear in the surface region 5 to 15 cm offshore of the shelf break. At the inshore side of the shear, the flow has considerable eddy activity, which is also seen farther onshore. Over the shelf itself is a much smaller velocity, which is again retrograde.

Some of the above flow may be driven by air drag. Consider that drag of air  $D_a$  on the surface of the water at radius  $r$  is approximately

$$D_a = \mu_a \Omega r / d_{ea}, \quad (2)$$

where  $\mu_a$  is the viscosity of the air,  $\Omega r$  is the differential speed between the air and the water, and  $d_{ea}$  is the Ekman Layer thickness  $= (\nu_a/f)^{1/2}$  where  $\nu_a$  is the kinematic viscosity of the air. This equals the Ekman drag on the bottom of the water on the shelf of magnitude  $\mu_w U / d_{ew}$ , where  $\mu_w$  is the viscosity of water,  $U$  is the drift velocity that is to be calculated, and  $d_{ew}$  is the thickness of the Ekman layer of the water  $(\nu_w/f)^{1/2}$  where  $\nu_w$  is the kinematic viscosity of the water. Equating these two leads to the formula

$$U = (\rho_a \mu_a)^{1/2} \Omega r / (\rho_w \mu_w)^{1/2} \quad (3)$$

Using the values  $\rho_a = 1.205 \times 10^{-3} \text{ gm/cm}^3$ ,  $\mu_a = 1.81 \times 10^{-4} \text{ gm/cm s}$ ,  $\rho_w = 0.998 \text{ gm/cm}^3$ , and  $\mu_w = 10^{-2} \text{ cm}^2/\text{s}$  (from Appendix I of Batchelor (1967)), this is approximately equal to  $0.005 \Omega r$ .

Eq. (3) gives drift velocity of  $0.13 \text{ cm/s}$  for  $f = 1 \text{ s}^{-1}$  and  $r = 50 \text{ cm}$ . For all the observations in this study, this wind driven velocity is much smaller than the observed velocities at the front near the shelf break. However, it is a little larger than the magnitude of the velocity on the shelf, and probably the drift current on the shelf is influenced by air drag.

#### 4. Heat Flow Measurements

To calculate heat flux, use was made of the transient nature of the experiment. Exploratory runs were conducted with thermistor locations shown by small numbers in Fig. 1, and final runs had locations shown by large numbers. Depth of water on the shelf was either 5, 10, or 20 cm.

Preliminary measurements of temperature as a function of time are shown in Fig. 3.

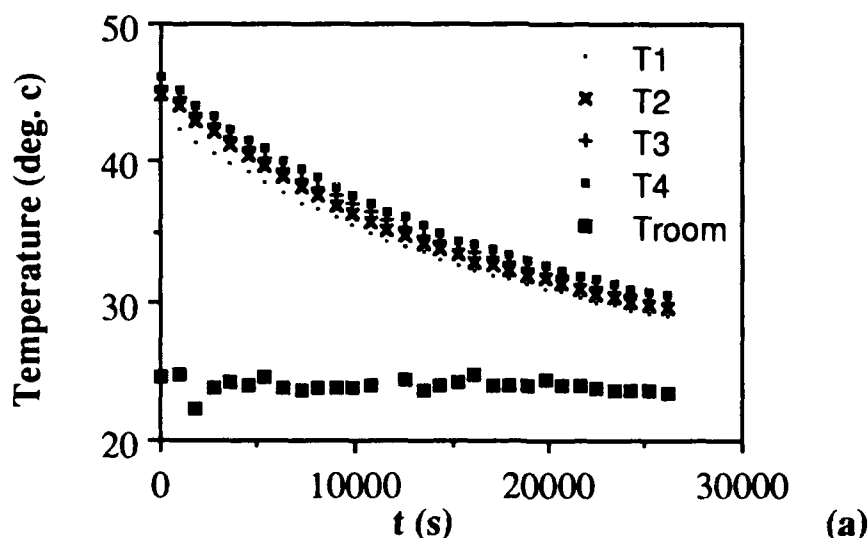


Figure 3 a. Centerline temperatures as a function of time for a typical exploratory experiment.  $T_n$  denotes the thermistor locations shown in Fig. 1.

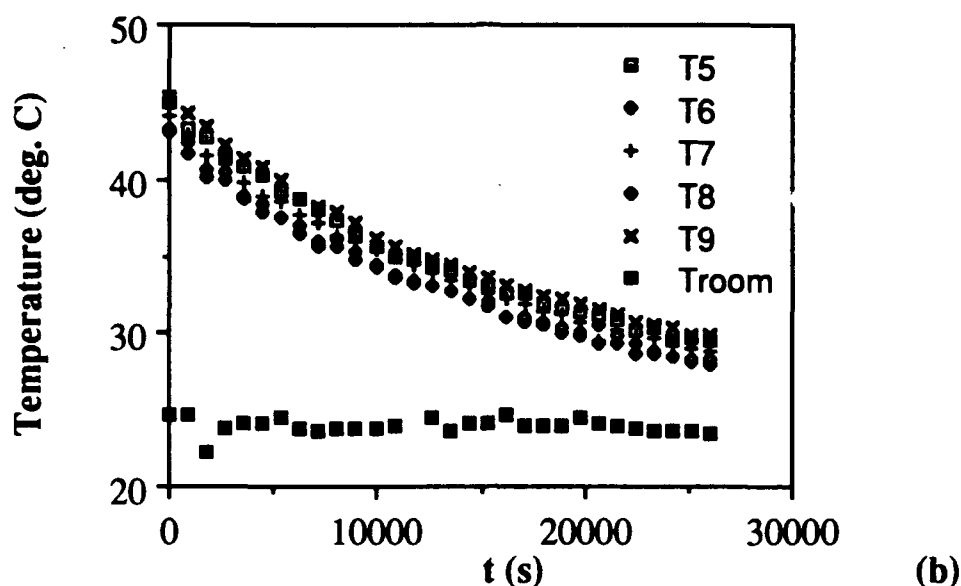


Figure 3 b. Shelf temperatures as a function of time for a typical exploratory experiment.  $T_n$  denotes the thermistor locations shown in Fig. 1.

It is clear that after an initial adjustment period of one to two hours, the temperatures at the different locations track each other closely and show a cooling response that looks like an exponential cooling curve. In some cases, the curves were so close to exponential that the time constant could be measured accurately by measuring the slope of the logarithm of the temperature difference between the water and the room. However, in other cases this did not work. Since there is no reason to expect that the curves would be exponential, other techniques were developed to analyze the data.

The heat flow (henceforth to be called  $H_n$ ) from the shelf to the deep basin across the shelf break was estimated from the data of temperature at location  $n$  (henceforth to be called  $T_n$ ) versus time using the formula  $H_n = \rho c_p V \partial T_n / \partial t$ , where  $\rho$  is density of water,  $c_p$  is heat capacity, and  $V$  is volume of the basin from the shelf break to the center. Using  $\rho = 1 \text{ gm/cm}^3$ ,  $c_p = 1 \text{ cal/ gm } ^\circ\text{C}$ ,  $V = 186,960$ ;  $230,585$ ; and  $317,835 \text{ cm}^3$  for the 5, 10 and 20 cm deep containers, respectively, and approximating  $\partial T_n / \partial t = \delta T_n / 900$  where  $\delta T_n$  is the change in temperature in 900 seconds, the formula for heat flow becomes

$$H_n = C_o \delta T_n \text{ cal/s.} \quad (4)$$

where the constant  $C_0 = 207.73, 256.19, \text{ and } 353.14 \text{ cal/s } ^\circ\text{C}$  is defined for the three depths. This calculation to estimate heat flux was performed on the entire set of readings of an individual thermistor for the duration of the experiment. Since the time derivative was found using the exact differences between sequential readings, the estimates of cooling versus time were much more irregular than the original temperature records. Thus the heat flux data were smoothed with a three point running mean to restore the smoothness of the original temperature series as a function of time.

By considering thermistor placement carefully and by comparison of results with other results in which the top lid had baffles, the data were determined with less ambiguity than the early analyses admitted. Clear lessons were learned about placement of the thermistors and which thermistor locations to use for a heat flux estimate. For example, temperature records of thermistors in locations 1-4 of the preliminary experiments, which were at the center of the basin and in locations 8 and 9 which were at the coast bottom were so smooth that cooling could be directly calculated by finite difference for each time step with small scatter about a visible trend. Unfortunately thermistors 3 and 4 near the top center of the tank took approximately 6000 to 8000 seconds after the experiments began to come to steady state, so important data near the beginning of the experiment were lost. In contrast, other records such as location 5 near the shelf break were not as smooth over time (almost certainly due to eddies) so that scatter of estimated cooling rate was great. However, it was found that smoothed data from location 5 were almost as good as the data from the central thermistors at later times.

Since Fig. 2 showed that temperature on the shelf at mid-depth extends continuously from the center of the tank to the shelf break, it proved to be difficult to define unambiguously a "typical" temperature difference between the shelf fluid and offshore. This was due to two features. The first is a large bowl shape to the isotherms in the deep basin from anticyclonic circulation of the "deep ocean". The second feature is a strong front at the shelf break. Originally, it had been thought that location 5 or 9 of the exploratory placement, which was located directly over the shelf break, would provide the measurement of offshore temperature. Unfortunately, both were extremely unsteady for almost all rotation rates. Sometimes the temperature was almost as cold as at T8 (shelf bottom next to coast wall). At other times it was as warm as offshore. Small injection of dye indicated that the flow was extremely complicated. For instance the cold events were

not due to cold eddies of bottom water but rather from water in a top mixed layer that had already been cooled by surface cooling.

In spite of the problems with clearly defined temperature difference, data giving temperature difference and heat flux were easily obtained. Fig. 4 shows one such set of measurements.

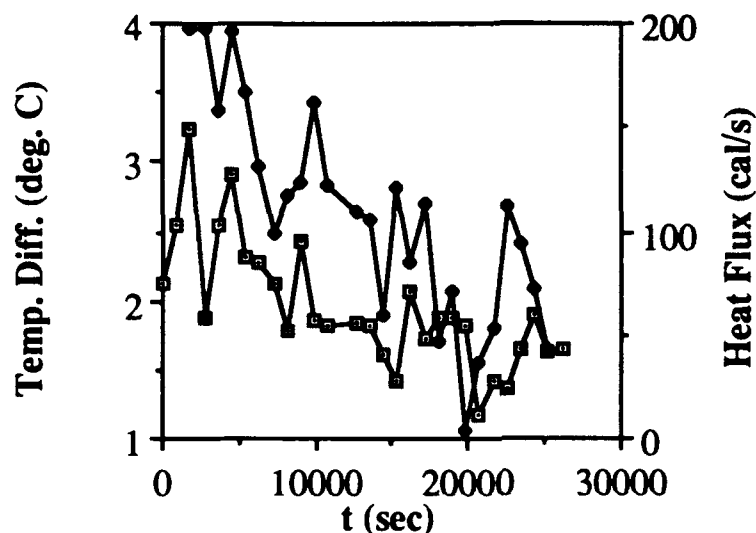


Figure 4. Measurements in the preliminary experiments of heat flow (solid dots) at location 4 with time and temperature difference between locations 8 and 9 (open squares) with time. Shelf depth  $h = 5$  cm,  $f = 1.000 \text{ s}^{-1}$ .

The array of thermistors was redesigned for the remaining experiments to produce a clearer picture of the temperature structure of the large offshore front. Only one thermistor was retained at the center of the tank at the top right under the insulating lid. In order to more clearly resolve the front at the shelf break, thermistors 2-6 were spaced offshore of the shelf at 2.5 cm depth so that #6 was at the shelf break and each lower numbered one was 2 cm farther offshore--toward the center of the tank. The new placement of thermistors is shown in bold numbers in Fig. 1.

The data from these showed that the question of estimating one typical offshore temperature had not yet been resolved. There was a large change in temperature offshore

of the shelf break compared to temperature change across the shelf itself. This is shown in the nine records of temperature versus time in Fig. 5a and in Fig. 5b for the thermistors offshore of the shelf at 2.5 cm depth.

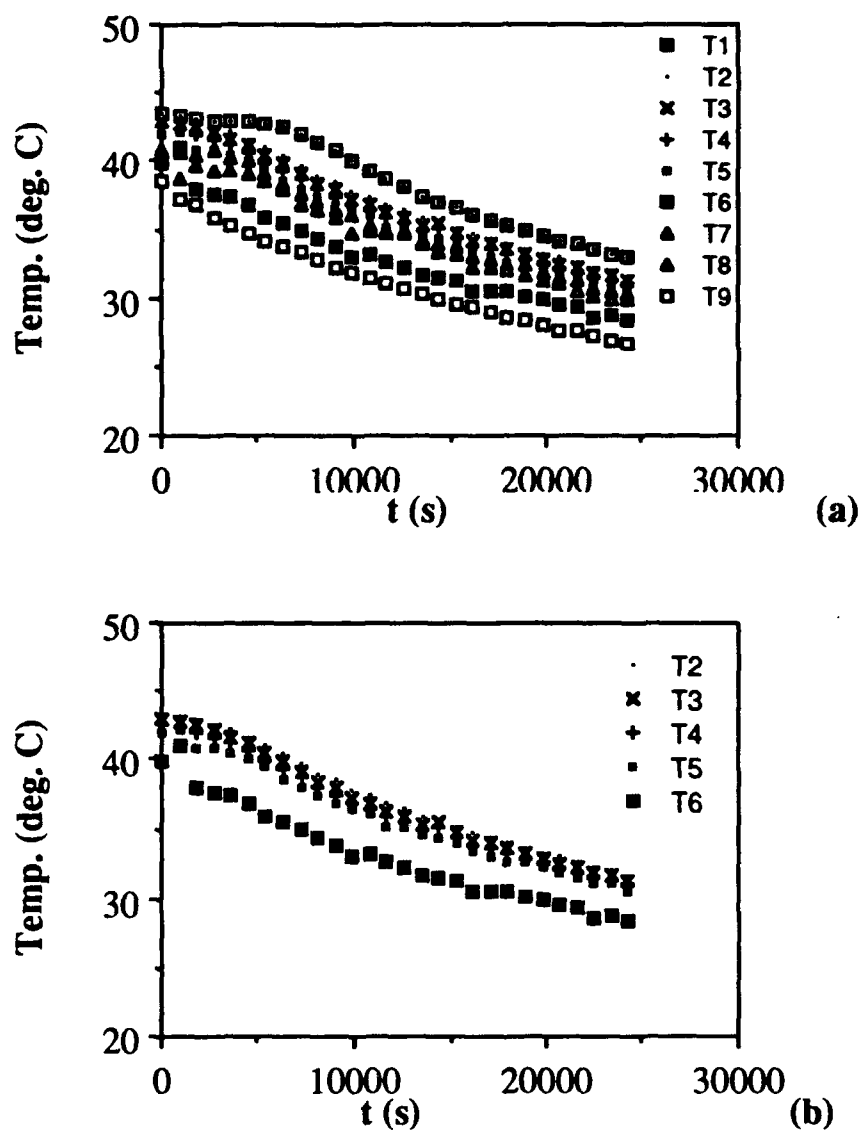


Figure 5. Temperature versus time for final thermistor placement. a) All 9 thermistors, b) Thermistors 2 through 6, which lie offshore of the front and maintain close to the same value in comparison to thermistor 9. Shelf depth  $h = 5$  cm,  $f = 1.000$  s $^{-1}$ .



Since it is important to define temperature difference between shelf and offshore, a number of possible measurements were considered. Henceforth difference between location "n" and  $T_9$  will be called  $D_n$ . Fig. 6 shows the difference between  $T_2$  through  $T_6$  and  $T_9$  (bottom inner shelf), and it is clear that difference varies strongly with location. Which of these pairs gave the most satisfactory measure of temperature difference was found by comparing these values with heat flux.

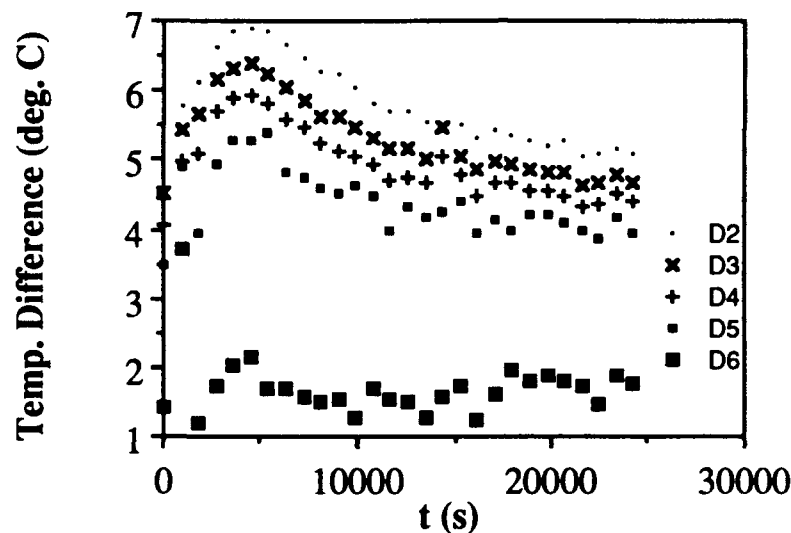


Figure 6. Temperature difference  $D_n$  between thermistors 2 through 6 and 9, versus time. Shelf depth  $h = 5$  cm,  $f = 1.000 \text{ s}^{-1}$ .

Heat flux was found using Eq. 4 for numerous thermistors in three runs, two with  $f = 1.000 \text{ s}^{-1}$ , and one with  $f = 0.5 \text{ s}^{-1}$ . It has already been described how the most useful estimates of heat flux were obtained from records where variability of consecutive readings was small. An illustration of this is shown in Fig. 7 where heat flux estimates from locations 2, 4, 5, 6 and 9 are shown. The results for the different thermistors lie on top of each other and show a small decrease with time.  $H_2$ , which is obtained using the thermistor closest to the center of the tank, had the least scatter by a wide margin.  $H_6$ , from over the shelf break, has enormous scatter from time variations. The scatter is greater for thermistors closer to the shelf break because the records are less steady, clearly due to baroclinic eddies in the strong front at the break. After some comparison between the

assorted records from the runs, it was felt the best estimates for heat flow were  $H_4$  and  $H_9$ .

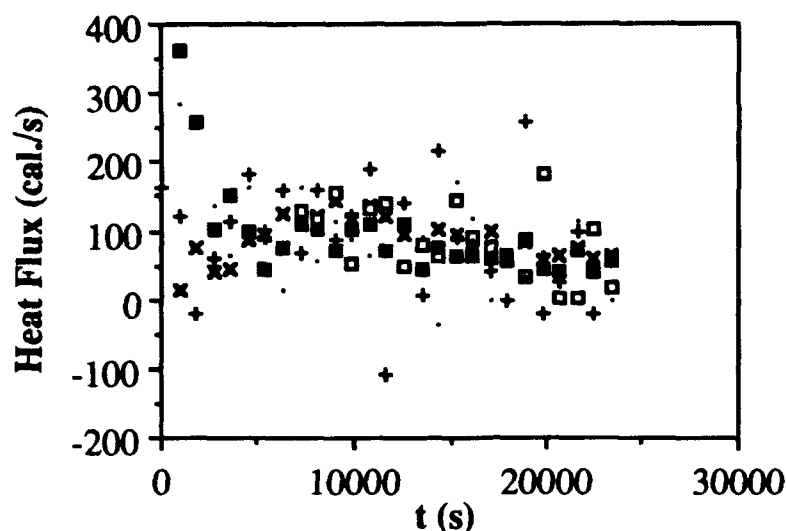


Figure 7. Heat flux estimates for thermistors 2, 4, 5, 6, and 9. Symbols for 2, 5 and 6 are x, + and ·, respectively. The values for  $H_4$  and  $H_9$ , which are the estimates used in the main study, are shown as open and closed squares, respectively.

The heat flux data were used to decide which thermistor pairs gave the best measure of temperature difference between the shelf fluid and offshore. To help in visualizing the features of various thermistor pairs,  $H_4$  is shown in Fig. 8 as a function of the values of  $D_n$ , the temperature difference between station  $n$  and 9, for new thermistor locations 2 through 6 and for two runs at rotation rates  $f=1 \text{ s}^{-1}$  and  $f=0.5 \text{ s}^{-1}$ . The records show that  $D_n$  decreases with heat flux in a coherent manner. For  $f=1.000 \text{ s}^{-1}$ ,  $D_2$  ranges from more than  $6^\circ\text{C}$  down to  $5^\circ\text{C}$  but for  $D_6$  this range is from  $2^\circ\text{C}$  to  $1^\circ\text{C}$ . For  $f=0.5 \text{ s}^{-1}$   $D_2$  ranges from  $4.5^\circ\text{C}$  down to  $2.6^\circ\text{C}$ , but for  $D_6$  this range is from  $1.2^\circ\text{C}$  to  $0.4^\circ\text{C}$ . Based on this, it was easy to exclude  $D_6$  from consideration, but which of the other values of  $D_n$  should be used was resolved by experiments with a baffled lid.

The problem of having such a spread in temperature difference arose because of both the front and the bowl shaped isotherms offshore of the shelf break. How much of the front arose from the large anticyclonic circulation, and how much would be there if the water offshore were stationary? Attempts were made to eliminate a significant portion of the offshore circulation and bowl shaped isotherms to see if the front would vanish. To accomplish this, a lid that had eight flow baffles underneath was made to cover the inner basin. These baffles were 15 cm deep and extended from the center to the shelf break, but

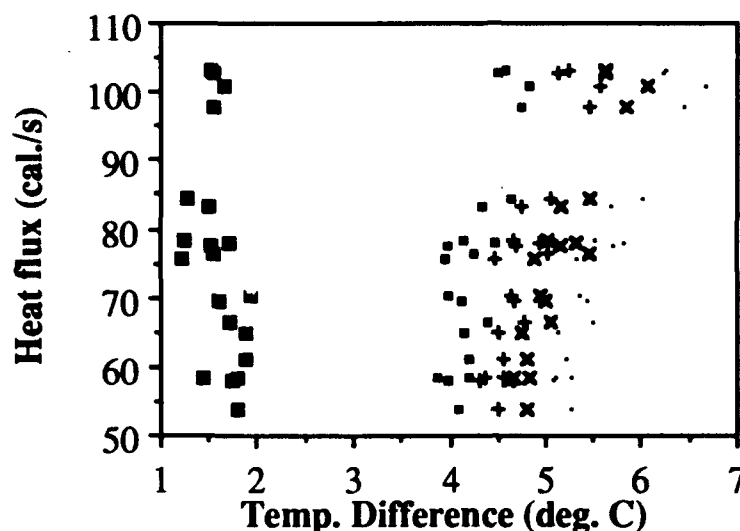


Figure 8. Heat flux versus temperature difference for thermistors 2 through 6. Symbols for thermistor pairs are the same as in Fig. 6.

they were sloped at their outer edge to remain 5 cm above the shelf slope. This made the offshore water stagnant (or at least with a velocity smaller than the shelf flushing velocities studied here) and therefore more like a typical ocean. The baffles also conducted heat vertically so that isothermal water covered the top 15 centimeters. They did not, however, eliminate the front over the shelf break which by virtue of its persistence even with the baffles, was found to be a major percentage of the overall shelf to offshore temperature drop. Fig. 7 shows records of  $D_n$  for  $n=1$  through 6 from the baffled experiment. The first four thermistors have almost identical temperatures. All were in the baffled region. Thermistors 5 (2 cm offshore of the break and 0.5 cm inshore of the baffle radius) and 6 (over the break) were cooler than thermistors 1-4 and indicate that there was still a front in this region.

A further comparison between baffled and nonbaffled is shown in figure 9. The nonbaffled experiments had more spread in temperature, but  $D_4$  and  $D_5$  have the same readings.

To compare the observations of the baffled experiments with the experiments where there was a fully developed front, running mean values of  $H_4$  and  $H_9$  as a function of the 9 point running mean of  $D_4$  and  $D_5$  were determined for both nonbaffled and baffled experiments at a rotation rate of  $f=0.5 \text{ s}^{-1}$ . Fig. 10 shows the results.

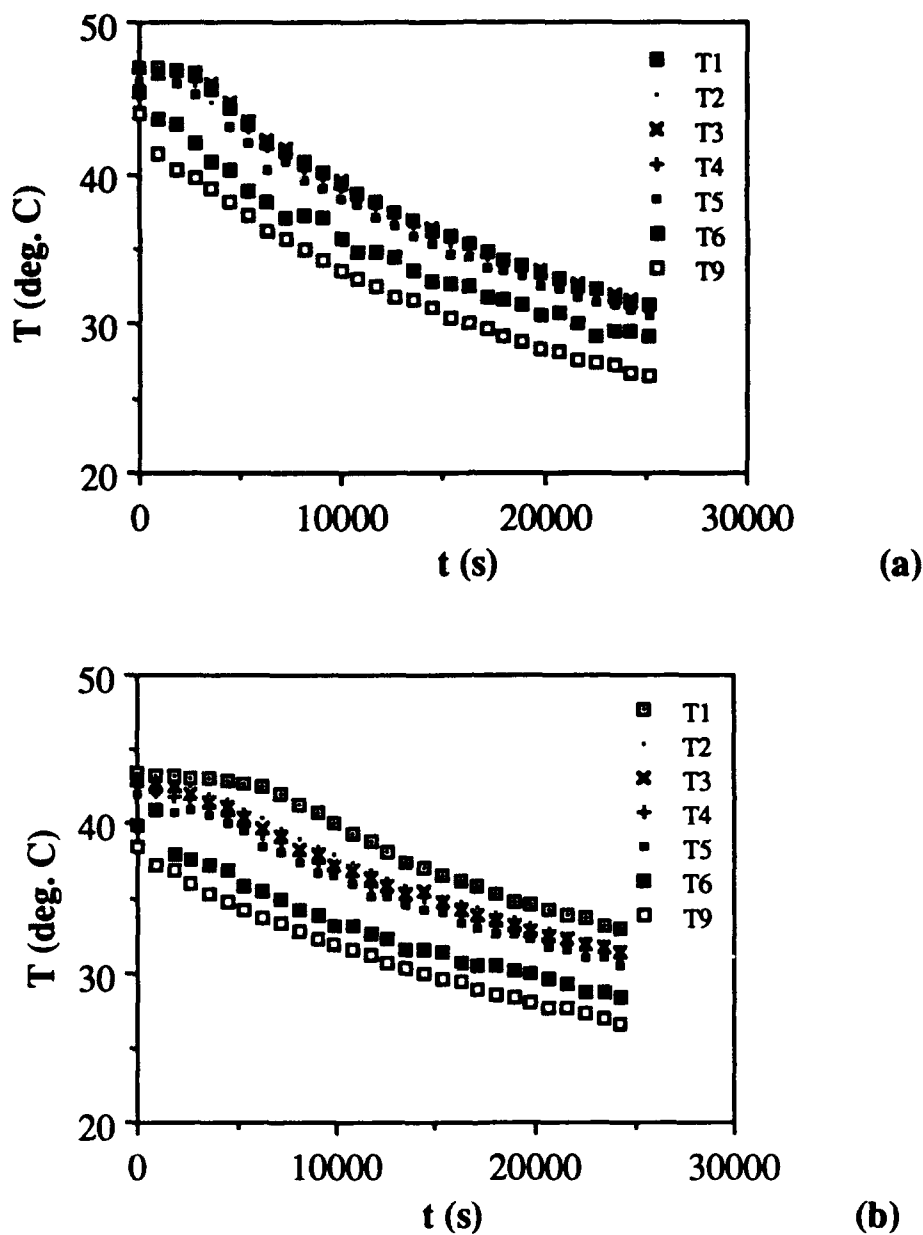


Figure 9. Temperature versus time for (a) baffled experiments and (b) otherwise identical nonbaffled experiments.

The data of heat flow and temperature difference lie almost completely over each other for both  $D_4$  and  $D_5$ . All four results appear to follow a linear relation between heat transfer and temperature difference, and the results for  $D_4$  are almost perfectly parallel to  $D_5$

but about 0.3°C higher. The temperature difference was not altered by the baffles, and we therefore conclude that the front was not eliminated by stopping the offshore flow.

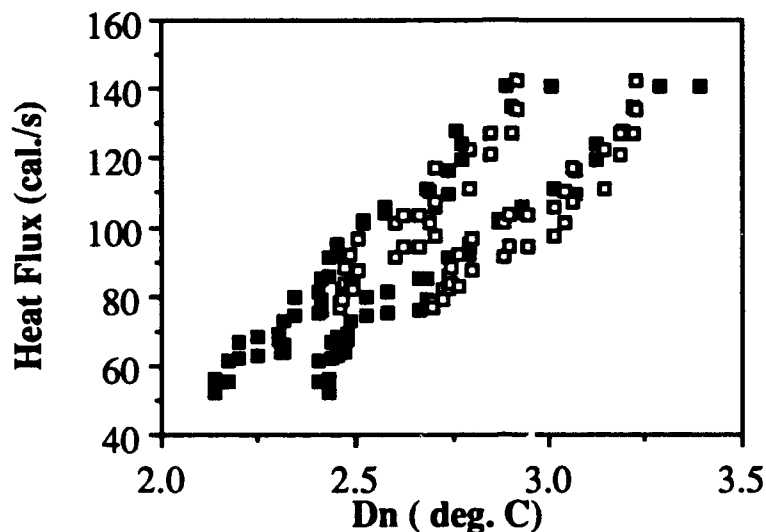


Figure 10. Heat flux versus  $D_4$  (right-hand cluster) and  $D_5$  (left-hand cluster) for the baffled results (open squares) and nonbaffled results (solid squares).

To compare quantitatively the baffled and nonbaffled results, the data in Fig. 10 were fit with best fit linear curves. All pairs of best fit curves for thermistors 4 and 5 are close to parallel, and the largest disagreement in temperature difference between baffled and nonbaffled results is approximately 5% of the value of the temperature difference at that point. Therefore, it was concluded that the elimination of the offshore front by the baffles had not altered the dynamics of the front and that the front must be included to link heat flow with temperature difference between fluid offshore of the shelf break and fluid on the shelf.

The close agreement between the baffled experiments and the ones with a strong offshore front also shows that the effects of the gradual temperature variation associated with the bowl-shaped isotherms can be largely neglected. It is safe to utilize only the records of  $D_4$  and  $D_5$  (mostly for redundancy) to estimate temperature difference between the coldest water on the shelf and offshore. At most, those two records differ by 25%, but in this study both are used for comparison with heat flow estimates.

These considerations have allowed measurements of heat transport and temperature difference that can be compared over a wide range of parameters. The preliminary experiments showed that offshore temperatures must only be recorded outside the sharp front at the shelf break, and all measurements were done under an insulated lid so that the mixed layer did not interfere with the temperature record.

It was desired to obtain data over a wide range of rotation rates, so experiments were conducted for rotation rates of  $f=1, 0.5, 0.25, 0.125, 0.063, 0.032, 0.016, 0.008$  and  $0 \text{ s}^{-1}$ . Each run lasted for approximately eight hours. Data were recorded every 15 minutes. The records for all nine thermistors were digitized so a view of the cooling in all the regions could be obtained.

The considerations given above resulted in using data from thermistors in the new locations 4 and 9 to calculate two values of heat flux, and using the differences between locations 4 and 9 and 5 and 9 to give two estimates of temperature difference between "shelf and ocean". Choice of these locations resulted from the recognition that more than 50% of the shelf to offshore temperature change happened at the offshore front. This was illustrated in the temperature records shown in Fig. 5. This was also illustrated in Fig. 10, which shows that the data with a baffled experiment are almost identical with those without the baffle. Finally, to eliminate some of the scatter, groups of 9 consecutive readings were averaged. Since every experiment had roughly 28 intervals of 15 minutes each over the eight hour period, this yielded three independent values of temperature difference and heat flux for each data string. Since two measurements were made of heat flux and two of temperature difference, each run resulted in 12 numbers.

The data of heat flux versus for  $D_4$  are shown in Figs. 11-14 for all the rotation rates that were used, and for fluid depths of 5 cm, 10 cm using both baffled and nonbaffled lids, and 20 cm with a nonbaffled lid. Clearly, temperature differences systematically increase both with increasing heat flow and with greater rotation rate. Thus the absolute value of temperature difference depends on position of the thermistor with respect to the offshore front, but the effect is less than 20% as big as that from changing rotation or fluid depth. Tabulated values are given in Tables 1-4.

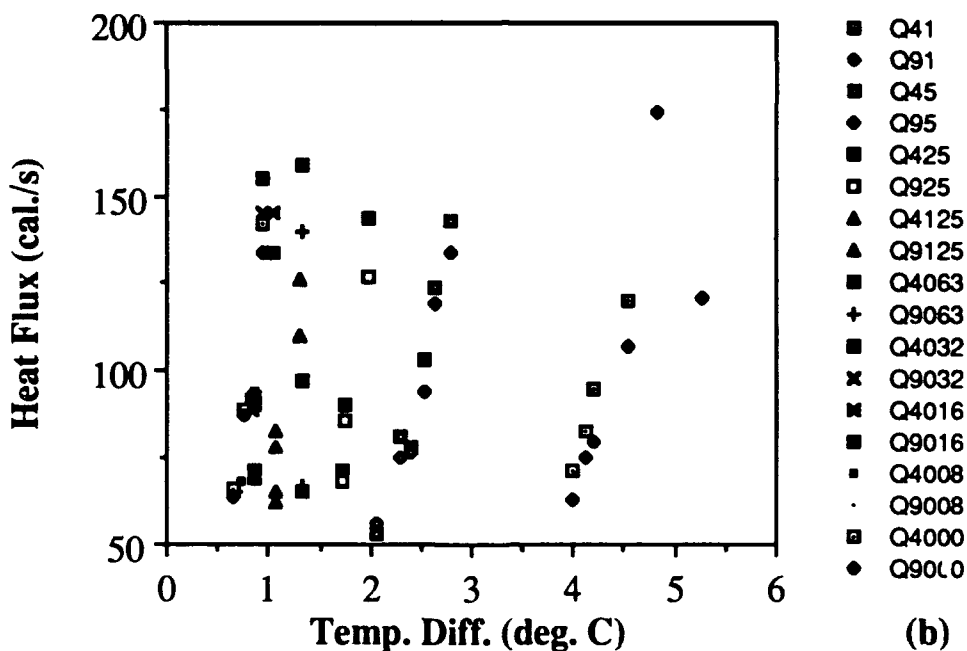
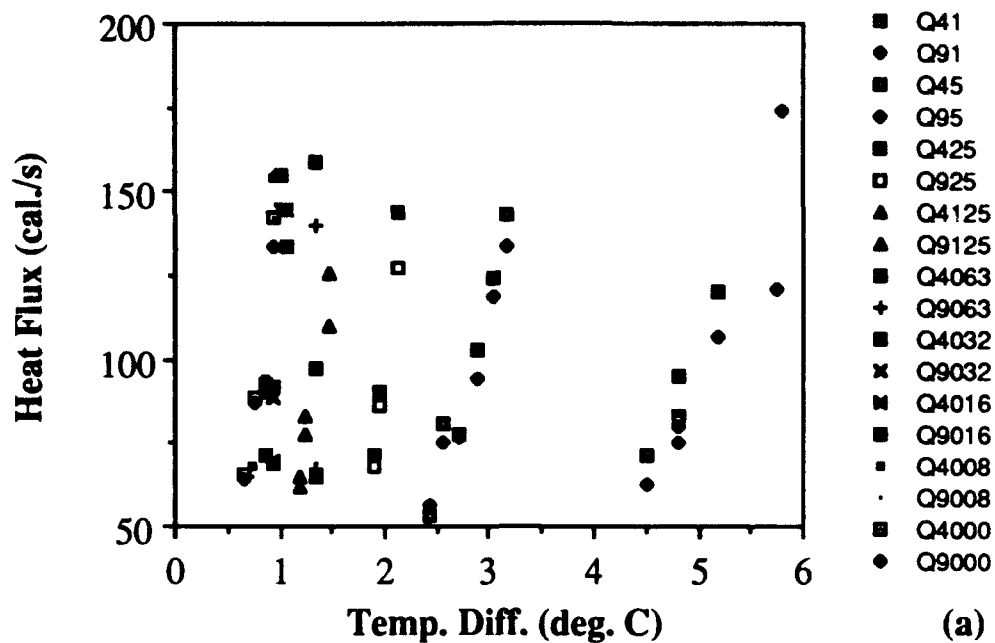


Figure 11. Heat flux versus temperature difference for the 5 cm deep experiments. (a) D4, (b) D5. The legend on the right contains codes to identify the data. The first number denotes whether H4 or H9 is indicated by this symbol. The next numbers denote the value of  $f$  with the decimal point left off. Thus "Q9032" indicates H9 was used and  $f=0.032 \text{ s}^{-1}$ .

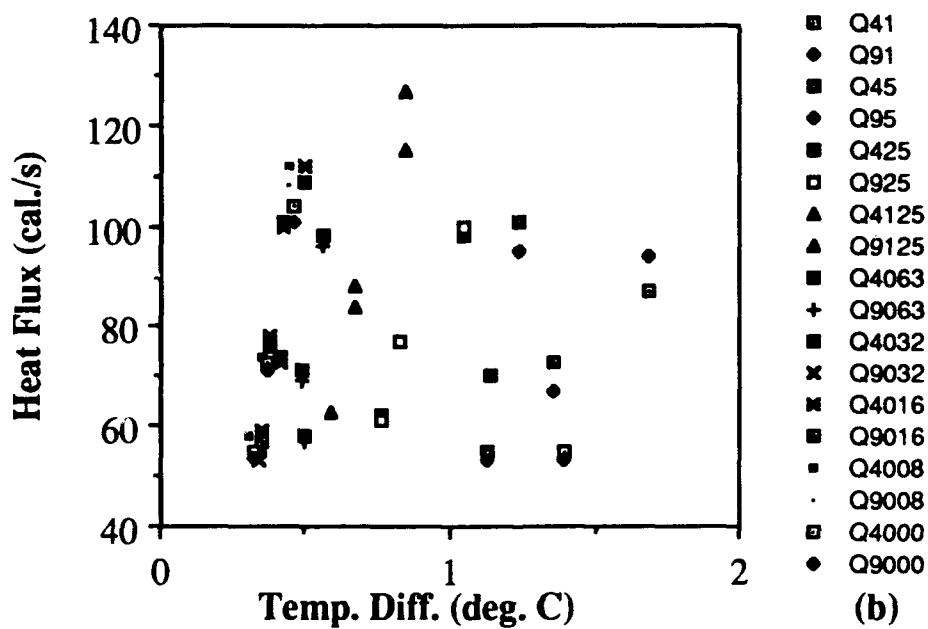
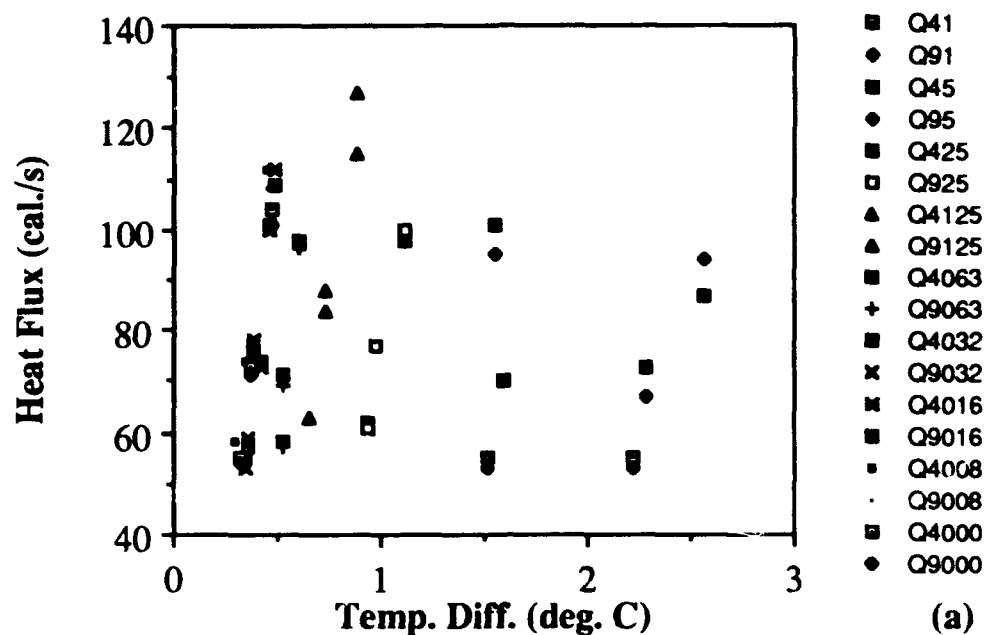


Figure 12. Heat flux versus temperature for experiments with a baffled lid and 10 cm depth. (a) D4 (b) D5. Codes on the right legend are the same as in Fig. 11.



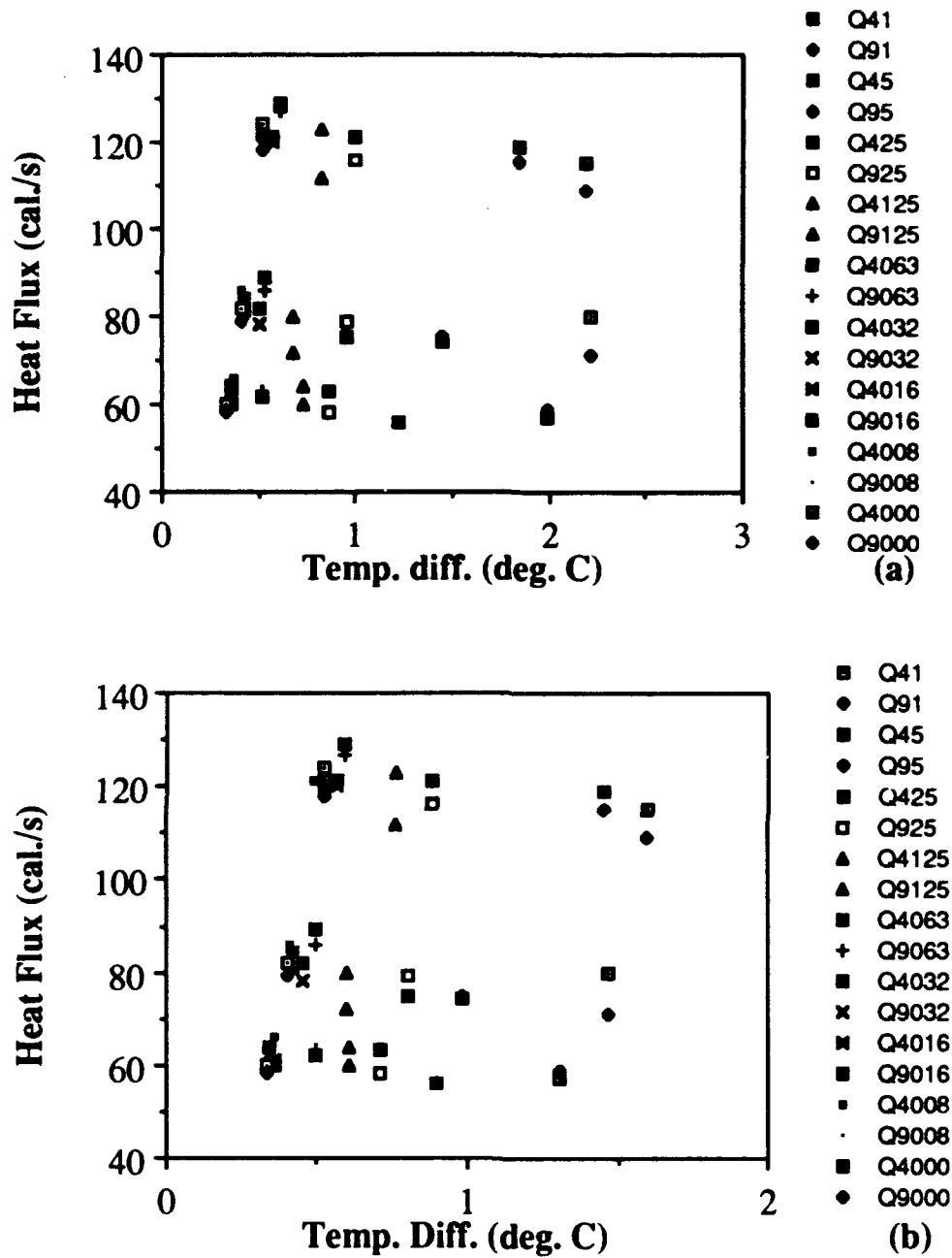


Figure 13. Heat flux versus temperature for experiments with a nonbaffled lid and 10 cm depth. (a) D4 (b) D5. Codes on the right legend are the same as in Fig. 11.

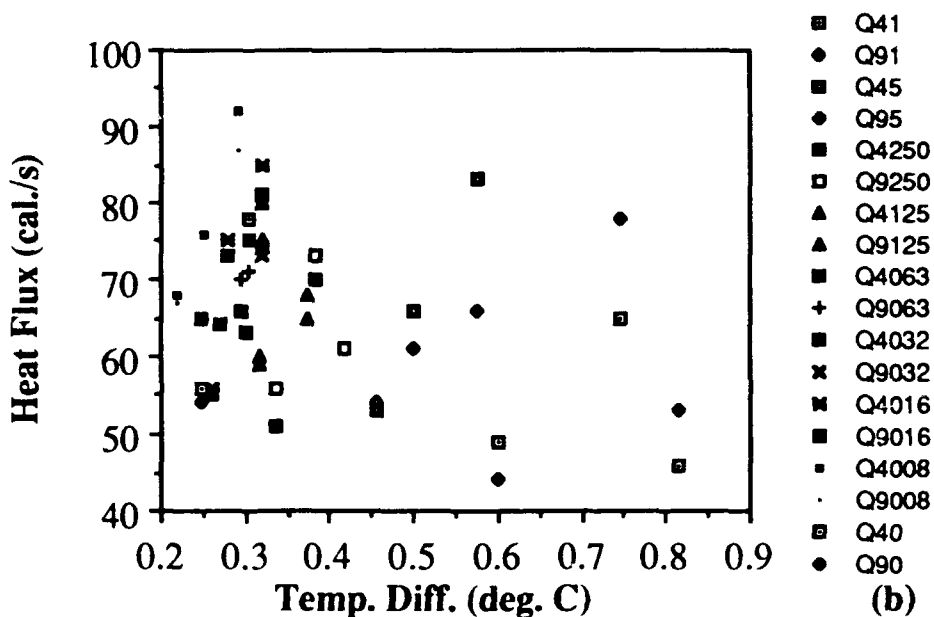
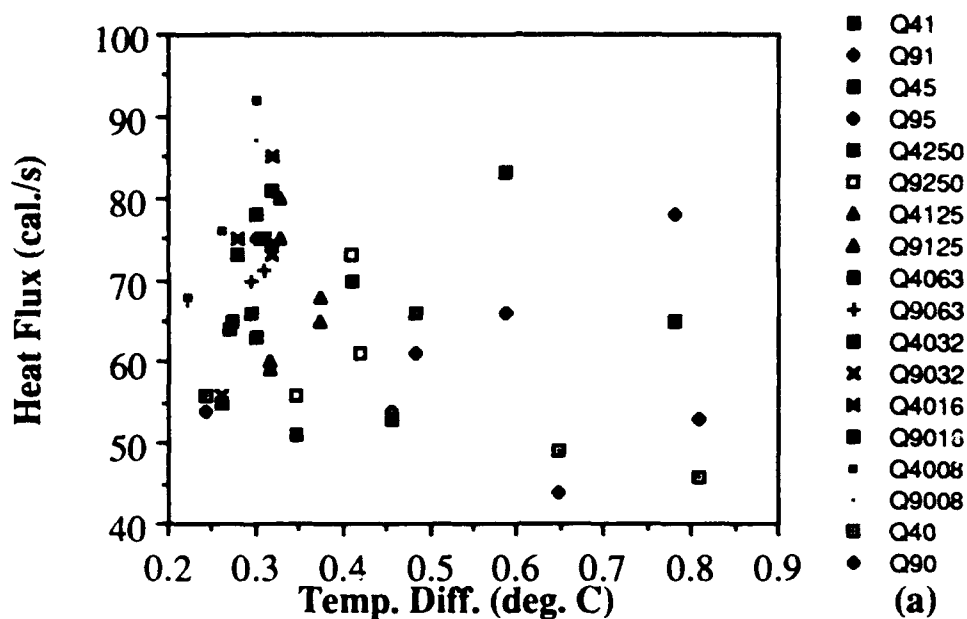


Figure 14. Heat flux versus temperature for experiments with a nonbaffled lid and 20 cm depth. (a) D<sub>4</sub> (b) D<sub>5</sub>. Codes on the right legend are the same as in Fig. 11.

Table 1. Rotation rate, temperature differences ( $^{\circ}\text{C}$ ) and heat flux (cal/s) for the 5 cm deep baffled experiments.

$f$	$D_4$	$D_5$	$H_4$	$H_9$
1.000	5.81	4.82		174
1.000	5.19	4.53	120	107
1.000	4.81	4.18	83	75
1.000	5.75	5.27		121
1.000	4.82	4.19	95	80
1.000	4.51	3.99	71	63
0.500	3.05	2.64	124	119
0.500	2.56	2.30	81	75
0.500	2.43	2.06	53	56
0.500	3.16	2.75	143	134
0.500	2.88	2.52	103	94
0.500	2.70	2.34	78	77
0.250	2.13	1.99	144	127
0.250	1.94	1.74	90	86
0.250	1.89	1.72	71	68
0.125	1.47	1.31	126	110
0.125	1.23	1.06	83	78
0.125	1.20	1.08	62	65
0.063	1.45	1.36	159	140
0.063	1.57	1.46	97	97
0.063	1.67	1.58	65	67
0.032	1.02	0.93	155	145
0.032	0.94	0.84	92	89
0.032	0.93	0.86	69	70
0.016	1.05	1.05	145	134
0.016	0.87	0.87	93	90
0.016	0.85	0.86	71	71
0.008	0.94	0.93	154	156
0.008	0.86	0.85	94	91
0.008	0.74	0.73	68	65
0	0.94	0.93	142	134
0	0.76	0.76	89	87
0	0.66	0.66	66	64

Table 2. Rotation rate, temperature differences ( $^{\circ}\text{C}$ ) and heat flux (cal/s) for the 10 cm deep baffled experiments.

f	$D_4$	$D_5$	$H_4$	$H_9$
1.000	2.57	1.69	87	94
1.000	2.28	1.36	73	67
1.000	2.22	1.39	55	53
0.500	1.55	1.24	101	95
0.500	1.59	1.14	70	70
0.500	1.50	1.13	55	53
0.250	1.12	1.05	98	100
0.250	0.98	0.83	77	77
0.250	0.93	0.76	62	61
0.125	0.88	0.84	127	115
0.125	0.73	0.67	88	84
0.125	0.66	0.59	63	63
0.063	0.60	0.56	98	96
0.063	0.52	0.49	71	69
0.063	0.52	0.50	58	57
0.032	0.46	0.42	101	100
0.032	0.42	0.41	74	73
0.032	0.35	0.34	55	53
0.016	0.49	0.50	112	109
0.016	0.39	0.38	78	76
0.016	0.36	0.35	59	57
0.008	0.45	0.44	112	108
0.008	0.35	0.35	74	72
0.008	0.30	0.30	58	56
0	0.48	0.46	104	101
0	0.37	0.37	73	71
0	0.32	0.32	55	54

Table 3. Rotation rate, temperature differences ( $^{\circ}\text{C}$ ) and heat flux (cal/s) for the 10 cm deep nonbaffled experiments.

$f$	$D_4$	$D_5$	$H_4$	$H_9$
1.000	2.19	1.60	115	109
1.000	2.22	1.47	80	71
1.000	1.99	1.31	57	59
0.500	1.85	1.45	119	115
0.500	1.45	0.98	74	75
0.500	1.22	0.90	56	56
0.250	0.99	0.88	121	116
0.250	0.95	0.80	75	79
0.250	0.86	0.71	63	58
0.125	0.82	0.76	123	112
0.125	0.68	0.60	72	80
0.125	0.73	0.61	64	60
0.063	0.61	0.59	129	127
0.063	0.53	0.50	89	86
0.063	0.52	0.50	62	63
0.032	0.57	0.56	121	120
0.032	0.50	0.45	82	87
0.032	0.36	0.34	64	62
0.016	0.53	0.52	120	121
0.016	0.43	0.42	84	81
0.016	0.36	0.36	61	60
0.008	0.50	0.49	121	121
0.008	0.41	0.41	86	85
0.008	0.37	0.36	66	65
0	0.52	0.52	124	118
0	0.40	0.40	82	79
0	0.33	0.33	60	58

Table 4. Rotation rate, temperature differences ( $^{\circ}\text{C}$ ) and heat flux (cal/s) for the 20 cm deer nonbaffled experiments.

$f$	$D_4$	$D_5$	$H_4$	$H_9$
1.000	0.78	0.75	65	78
1.000	0.81	0.81	46	53
1.000	0.65	0.60	49	44
0.500	0.59	0.58	83	66
0.500	0.48	0.50	66	61
0.500	0.46	0.45	53	54
0.250	0.41	0.38	70	73
0.250	0.42	0.42	61	61
0.250	0.35	0.34	51	56
0.125	0.33	0.32	75	80
0.125	0.37	0.37	65	68
0.125	0.32	0.32	59	60
0.063	0.31	0.30	75	71
0.063	0.30	0.30	66	70
0.063	-	-	-	-
0.032	0.32	0.32	74	73
0.032	0.30	0.30	63	63
0.032	0.26	0.26	55	56
0.016	0.32	0.32	85	81
0.016	0.28	0.28	75	73
0.016	0.27	0.27	64	64
0.008	0.30	0.29	92	87
0.008	0.26	0.25	76	76
0.008	0.22	0.22	68	87
0	0.30	0.30	78	75
0	0.27	0.27	65	65
0	0.24	0.25	56	54

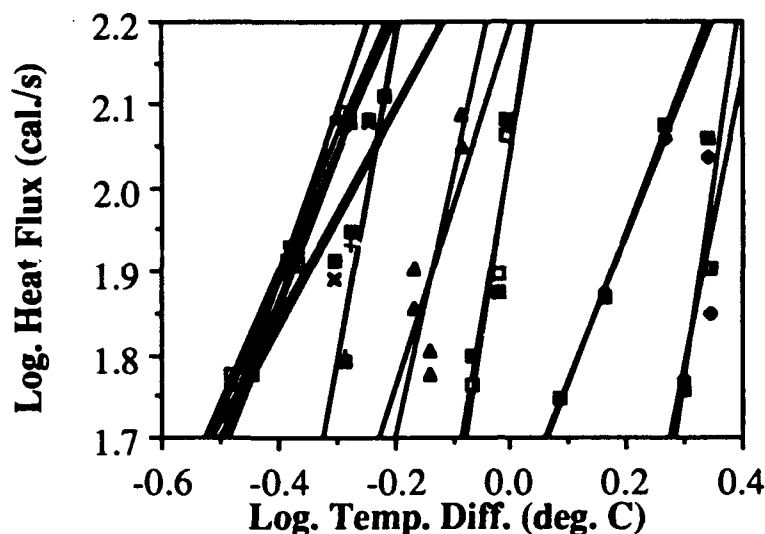


Figure 15. Best fit lines for data shown in Fig. 13b.

It was not obvious how to analyze the data further. An example of an attempt to fit to power laws (without useful results) is shown in Fig. 15. Slopes were found for all data but there was wide scatter between values of slope and the information was of limited value. However, there were some clear trends. First, at rotation rates of roughly 0.032 and less the heat flux as a function of temperature difference approached a log-log power law of  $3/2$ . Second, the fastest rotation rates had a clearly greater power law, possibly up to a power of 3, although scatter is great. These trends were visible both with 10 cm and 20 cm experiments.

A better view was found by first noting that all results had heat flow of approximately 100 cal/s for the first time interval. Assuming that these results have fixed heat flow, temperature difference at the first time interval can be plotted as a function of  $f$ . An example is shown in Fig. 16. It illustrates the effect of rotation on the temperature difference for fixed heat flow. At low and zero rates of rotation as shown to the left, temperature difference has a constant value that is unaffected by rotation. For approximately  $f > 0.1 \text{ s}^{-1}$ , temperature difference increases with  $f$ . At the largest value, the slope of temperature difference with  $f$  gets close to 1 on a log-log plot.

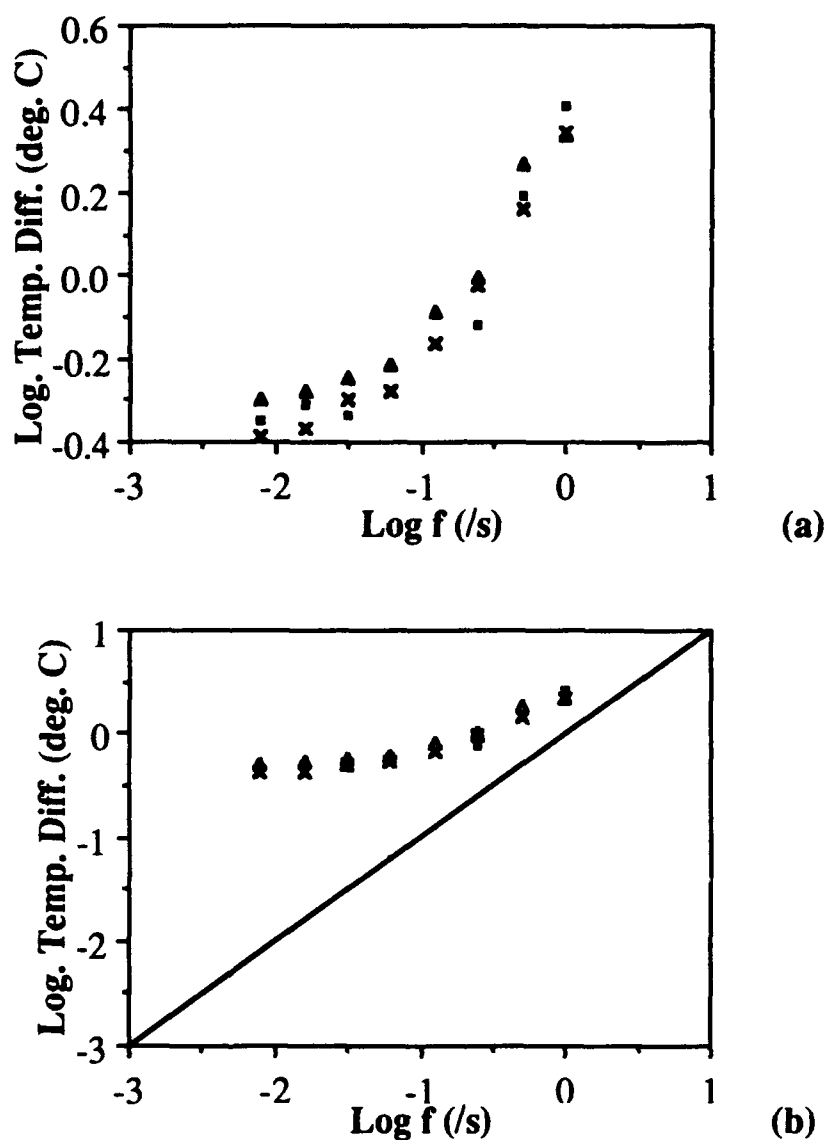


Figure 16. Temperature difference versus rotation rate for experiments with heat flux of approximately 100 cal/s and 10 cm depth. The triangles identify nonbaffled experimental data, the squares indicate baffled data, and the x shows the middle heat flux reading from the nonbaffled experiment. (a) Close-up of the result in log-log space. (b) The same data compared to a line with a slope of 1.

Inspection of all the data in Figs. 11-14 revealed that there was consistency with the notion that temperature difference is inversely proportional to depth  $h$ , proportional to heat



flux to the  $2/3$  power for low rotation, to the  $1/3$  power law for fast rotation and may be approaching a power law of  $f^1$  for fast rotation. Motivated by this, a test was developed to determine whether heat flux data can be used to predict a temperature difference (henceforth called  $DT_h$ ) by the relation

$$DT_h = \frac{c_1 (H_n^{2/3})}{h} + \frac{c_2 f (H_n^{1/3})}{h}. \quad (5)$$

Theoretical justification for the values of the two exponents in Eq. (5) will be discussed in the next section. Values of  $c_1$  were found by least squares fit for each individual series of runs with the same depth, so that the three values of temperature at zero rotation agree with  $DT_h$ . Values of  $c_1$  were 0.186 for both  $D_4$  and  $D_5$  with 5 cm depth, 0.18 for both  $D_4$  and  $D_5$  for the baffled cases with 10 cm depth, 0.21 for  $D_4$  and 0.22 for  $D_5$  for the nonbaffled cases with 10 cm depth, and 0.08 for both  $D_4$  and  $D_5$  with 20 cm depth. Note that the values for the first six cases are close to 0.2. In contrast, the experiment with 20 cm depth had a significantly different constant of  $c_2=0.08$ . However, for that depth the ratio of width to depth is 1.5, which is small. Moreover, most of the runs were in the rapidly rotating limit, so we believe the coefficient value of 0.08 is less well established than the others. The value  $c_2=5$  fits all data nicely.

Using Eq. (5), values of  $DT_h$  were calculated using  $c_1=0.2$ ,  $c_2=5$ , and values of  $H_n$ ,  $f$  and  $h$  for each run. These are plotted against  $D_4$  and  $D_5$  in Fig. 17a and as log-log plots in 17b and c. All reveal a linear relation between the prediction and measurement, so there is surprisingly close agreement between eq. 6 and the measured temperature difference. The correlation coefficients are more than 0.99, and the slope of the log-log best fit is within 1% of 1.0. In Fig. 17b the two values of  $D_4$  and  $D_5$  are visible as two elongated trends in the data that are offset by less than 20% over a range of more than a factor of ten. This implies that the choice of the exact location of the thermistor offshore of the front is not central to this comparison, since the offset is small compared to the span of the entire results. Fig. 17c shows only the  $D_4$  data but each depth has different symbols. It reveals that the 5 and 10 cm results lie along the same line and show considerable overlap, but the 20 cm runs have slightly bigger values of  $DT_h$ .

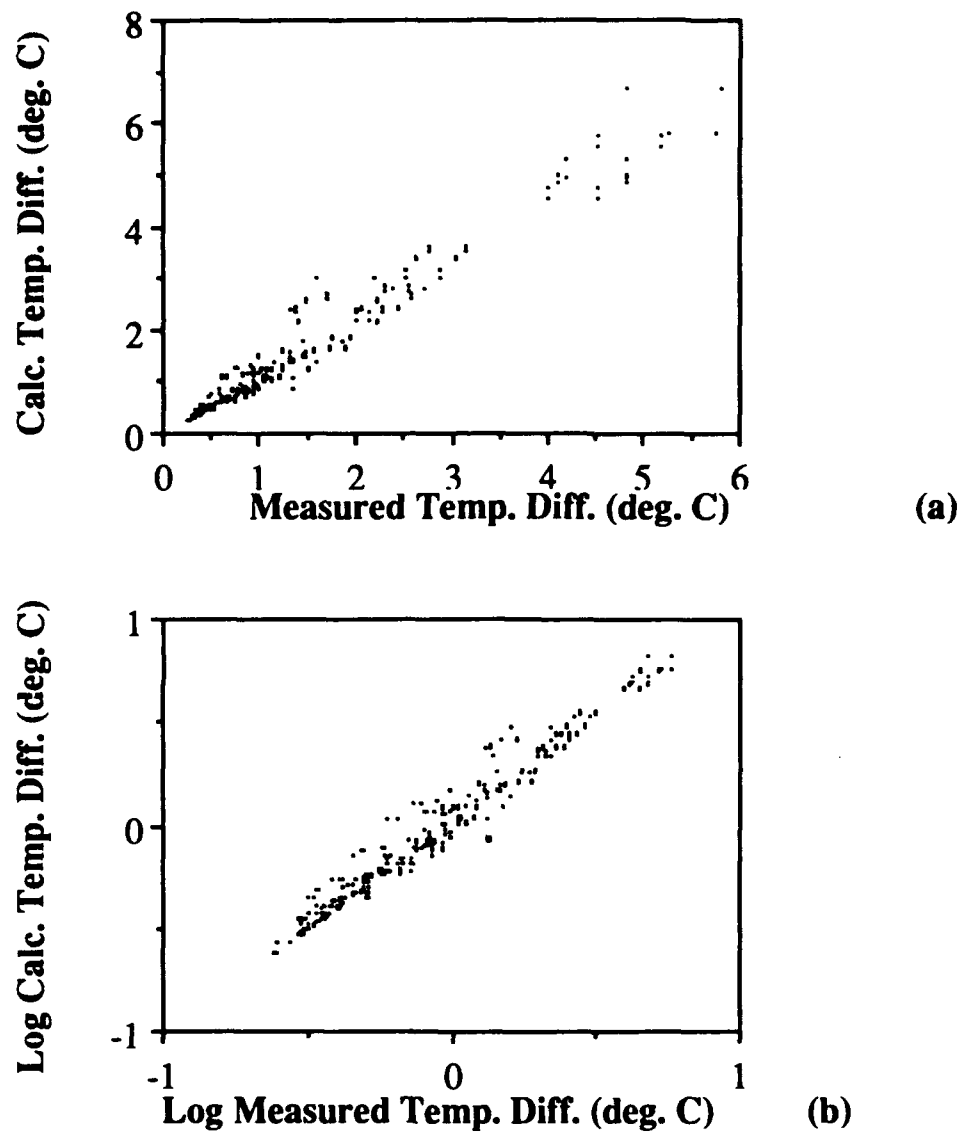


Figure 17. a. All measured values of  $D_4$  and  $D_5$  versus  $DT_h$ . b. The same in logarithmic scale.

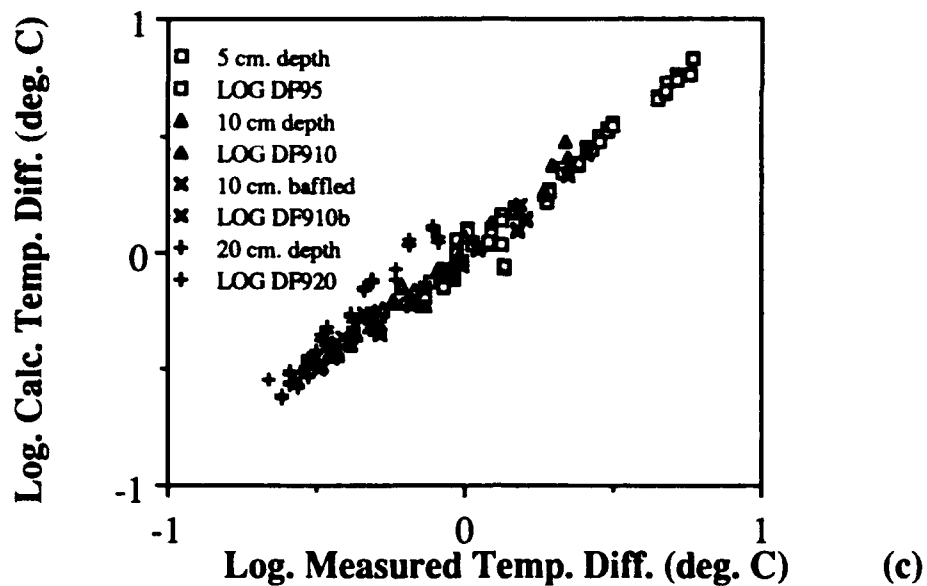


Figure 17c. The same as b, but for only D<sub>4</sub> and with each depth denoted by a different symbol.

To demonstrate that each of the terms in Eq. (5) is insufficient alone, Fig. 18 shows the values of each of the two terms (along with their sum) in comparison with the measured value of temperature. This calculation is done for the 10 cm deep experiments. It is clear that neither term alone has satisfactory comparison with the measured data over the entire range of rotation rates.

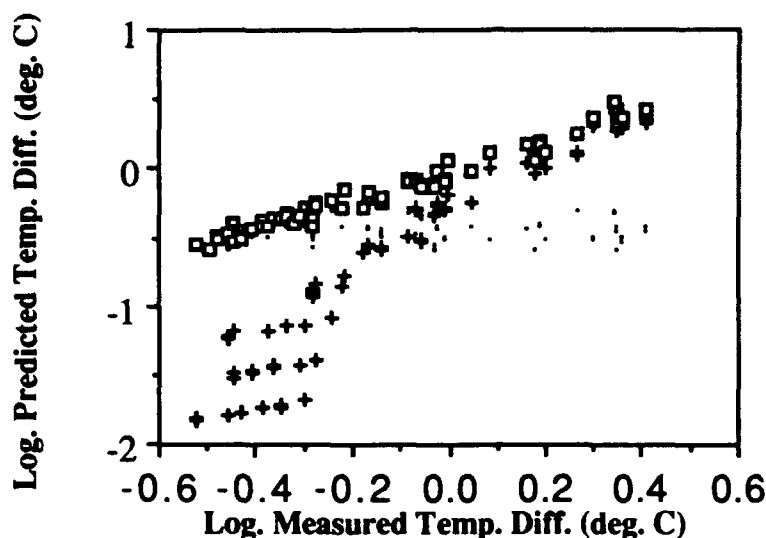


Figure 18. Measured values of  $D_4$  and  $D_5$  versus predicted values from heat flow measurements. The data shown as very small dots use the zero rotation term  $c_1 H_n^{2/3}/h$  for predicted temperature difference. The data shown as small rectangles use the rotation term  $c_2 f H_n^{1/3}/h$  for predicted temperature difference. The sum of these two terms corresponds to equation (6) and is shown as open squares. These are included in the data shown in Fig. 17. All data from the 10 cm deep experiments were used for this figure.

Eq. (5) almost collapses the data to a line over the entire range of rotation rates, for all three values of  $h$  used, and over a range of a factor of two for heat flux. The data with depths of 5 and 10 cm form the best trend that lends strong confirmation to Eq. 5. The data for 20 cm overlap the left-hand end of the data set but alone would not be consistent with a slope of 1. Although the value of the constant  $c_1$  for 20 cm was less than half the value for the other depths, this fit was not strongly affected for  $c_1$  over most of the range. Therefore, in view of the wide range of rotation rates, depths, and heat fluxes, and the small aspect ratio for the 20 cm data, it seems that Eq. 6 agrees with the data quite well. This is the principal result of the experiment.

## Acknowledgments

Suggestions by Glen Gawarkiewicz, Karl Helfrich, and Dave Chapman are gratefully acknowledged. Woods Hole Oceanographic Institution Contribution Number for the text accepted for publication in the Journal of Physical Oceanography is 8059.

## References

- Armi, L., 1986: The hydraulics of two flowing layers with different densities. *J. Fluid Mech.* 163, 27-58.
- Batchelor, G. K., 1967: *An Introduction to Fluid Dynamics*, Cambridge University Press, New York, 615pp.
- Brocard, D. N. and D. R. F. Harleman, 1980: Two-layer model for shallow horizontal convective circulation. *J. Fluid Mech.* 100, 129-146.
- Brocard, D. N., G. H. Jirka and D. R. F. Harleman, 1977: A model for convective circulation in side arms of cooling lakes. Ralph M. Parsons Laboratory for Water Resources and Hydrodynamics, Tech. Rept. 223, Department of Civil Engineering, Massachusetts Institute of Technology 270pp.
- Bryden, H. L. and H. M. Stommel, 1984: Limiting processes that determine basic features of the circulation in the Mediterranean Sea. *Oceanologica Acta*, 7, 289-296.
- Csanady, G. T., 1976: Mean circulation in shallow seas. *J. Geophys. Res.* 81, 5389-5399.
- Endoh, M., 1977: Formation of thermohaline front by cooling of the sea surface and inflow of the fresh water. *J. Oceanog. Soc. Japan* 33, 6-15.
- Farmer, D. M. and L. Armi, 1986: Maximal two-layer exchange over a sill and through the combination of a sill and contraction with barotropic flow. *J. Fluid Mech.* 164, 53-76.
- Fultz, D., 1961: Developments in controlled experiments on larger scaled geophysical problems. *Advanced Geophysics* 7, 1-103.
- Hide, R. and P. J. Mason, 1975: Sloping convection in a rotating fluid. *Advances in Physics* 24, 47-100.

Killworth, P. D., 1974: A baroclinic model of motions on Antarctic continental shelves. *Deep Sea Res.* 21, 815-837.

Killworth, P. D., 1977: Mixing on the Weddell Sea continental slope. *Deep Sea Res.* 24, 427-448.

Kowalik, Z. and J. B. Matthews, 1983: Numerical study of the water movement driven by brine rejection from nearshore Arctic ice. *J. Geophys. Res.* 88, 2953-2958.

Stommel, H. and H. G. Farmer, 1952a: Abrupt change in width in two-layer open channel flow. *J. Mar. Res.* 11, 205-214.

Stommel, H. and H. G. Farmer, 1952b: Control of salinity of an estuary by a transition. *J. Mar. Res.* 12, 13-20.

Stommel, H. and A. Leetmaa, 1972: The circulation on the continental shelf. *Proc. Nat. Acad. Sci.* 69, 3380-3384.

Sugimoto, T. and J. A. Whitehead, 1983: Laboratory models of bay-type continental shelves in the winter. *J. Phys. Oceanog.*, 13, 1819-1828.

Whitehead, J. A., M. E. Stern, G. R. Flierl and B. Klinger, 1990: Experimental observations of baroclinic eddies on a sloping bottom. *J. Geophys. Res.* 95, 9585-9610.

Whitehead, J. A., Jr., 1981: Laboratory models of circulation in shallow seas. *Phil. Trans. Royal Soc. London, A*, 302, 583-595.

Whitehead, J. A., 1993: A laboratory model of Cooling over the Continental shelf, *J. Phys. Oc.* In press.

Wood, I. R., 1970: A lock exchange flow. *J. Fluid Mech.* 42, 671-687.

Yih, C. S., 1980: *Stratified Flows*, Academic Press, New York, 418 pp.

## DOCUMENT LIBRARY

*Distribution List for Technical Report Exchange - July 1, 1993*

University of California, San Diego  
SIO Library 0175C (TRC)  
9500 Gilman Drive  
La Jolla, CA 92093-0175

Hancock Library of Biology & Oceanography  
Alan Hancock Laboratory  
University of Southern California  
University Park  
Los Angeles, CA 90089-0371

Gifts & Exchanges  
Library  
Bedford Institute of Oceanography  
P.O. Box 1006  
Dartmouth, NS, B2Y 4A2, CANADA

Office of the International Ice Patrol  
c/o Coast Guard R & D Center  
Avery Point  
Groton, CT 06340

NOAA/EDIS Miami Library Center  
4301 Rickenbacker Causeway  
Miami, FL 33149

Library  
Skidaway Institute of Oceanography  
P.O. Box 13687  
Savannah, GA 31416

Institute of Geophysics  
University of Hawaii  
Library Room 252  
2525 Correa Road  
Honolulu, HI 96822

Marine Resources Information Center  
Building E38-320  
MIT  
Cambridge, MA 02139

Library  
Lamont-Doherty Geological Observatory  
Columbia University  
Palisades, NY 10964

Library  
Serials Department  
Oregon State University  
Corvallis, OR 97331

Pell Marine Science Library  
University of Rhode Island  
Narragansett Bay Campus  
Narragansett, RI 02882

Working Collection  
Texas A&M University  
Dept. of Oceanography  
College Station, TX 77843

Fisheries-Oceanography Library  
151 Oceanography Teaching Bldg.  
University of Washington  
Seattle, WA 98195

Library  
R.S.M.A.S.  
University of Miami  
4600 Rickenbacker Causeway  
Miami, FL 33149

Maury Oceanographic Library  
Naval Oceanographic Office  
Stennis Space Center  
NSTL, MS 39522-5001

Library  
Institute of Ocean Sciences  
P.O. Box 6000  
Sidney, B.C. V8L 4B2  
CANADA

Library  
Institute of Oceanographic Sciences  
Deacon Laboratory  
Wormley, Godalming  
Surrey GU8 5UB  
UNITED KINGDOM

The Librarian  
CSIRO Marine Laboratories  
G.P.O. Box 1538  
Hobart, Tasmania  
AUSTRALIA 7001

Library  
Proudman Oceanographic Laboratory  
Bidston Observatory  
Birkenhead  
Merseyside L43 7 RA  
UNITED KINGDOM

IFREMER  
Centre de Brest  
Service Documentation - Publications  
BP 70 29280 PLOUZANE  
FRANCE

<b>REPORT DOCUMENTATION PAGE</b>	<b>1. REPORT NO.</b> WHOI-93-22	<b>2.</b>	<b>3. Recipient's Accession No.</b>
<b>4. Title and Subtitle</b> A Laboratory Model of a Cooled Continental Shelf			<b>5. Report Date</b> June 1993
			<b>6.</b>
<b>7. Author(s)</b> J.A. Whitehead and Robert E. Frazel			<b>8. Performing Organization Rept. No.</b> WHOI-93-22
<b>9. Performing Organization Name and Address</b>  Woods Hole Oceanographic Institution Woods Hole, Massachusetts 02543			<b>10. Project/Task/Work Unit No.</b>
			<b>11. Contract(C) or Grant(G) No.</b> (C) N00014-89-J-1037 (G)
<b>12. Sponsoring Organization Name and Address</b>  Office of Naval Research			<b>13. Type of Report &amp; Period Covered</b> Technical Report
			<b>14.</b>
<b>15. Supplementary Notes</b>  This report should be cited as: Woods Hole Oceanog. Inst. Tech. Rept., WHOI-93-22.			
<b>16. Abstract (Limit: 200 words)</b>  A laboratory model of wintertime cooling over a continental shelf has a water surface cooled by air in an annular rotating tank. A flat shallow outer "continental shelf" region is next to a conical "continental slope" bottom and a flat "deep ocean" center. The shelf flow consists of cellular convection cells descending into a region with very complicated baroclinic eddies. Extremely pronounced fronts are found at the shelf break and over the slope. Associated with these are sizable geostrophic currents along the shelf and over shelf break contours. Eddies are particularly energetic there. Cooling rate is compared with temperature difference between "continental shelf" and "deep ocean". Scaling considerations produce an empirical best fit formula for temperature difference as a function of cooling rate. This produces a relatively straight regression line over a wide range of rotation rates, shelf depths and cooling rates. If this formula is valid for the ocean, water over continental shelves will be much colder due to constraints imposed by rotation of the earth than if the fluid were not rotating.			
<b>17. Document Analysis</b> <b>a. Descriptors</b> cooled shelf continental shelf laboratory model convection  <b>b. Identifiers/Open-Ended Terms</b>          <b>c. COSATI Field/Group</b>			
<b>18. Availability Statement</b>  Approved for public release; distribution unlimited.		<b>19. Security Class (This Report)</b> UNCLASSIFIED	<b>21. No. of Pages</b> 40
		<b>20. Security Class (This Page)</b>	<b>22. Price</b>